The hunt for frozen organic molecules in space: a laboratory approach

Gomes Rachid, M.

1

Introduction

The first interstellar molecule was detected in 1937 (Swings and Rosenfeld, 1937). This molecule, the methylidyne radical (CH), was identified through its characteristic absorption of visible light. In the following years, other diatomic molecules were also identified, and to date, over 250 molecules have been detected in the interstellar medium (ISM), circumstellar environments, and extragalactic sources (see McGuire 2022 for a review). The majority of the molecules discovered in space were detected through their characteristic absorption and emission of light, which compose a spectral signature of every species. The identification of these signatures has become possible due to extensive laboratory measurements investigating the interactions between light and matter, the basis of spectroscopy. Comparing astronomical observations with the spectra of molecules recorded under simulated interstellar environments allows for identifying molecular species in space and at the same time to obtain information about the physical conditions in their surroundings. The energy level distribution of a molecule and its absorption and emission line profiles are dependent on the temperature, density, radiation field, and kinematics of the medium. Thus, the detection and analysis of molecular features also provide a gauge of interstellar conditions. This thesis focuses on the laboratory spectroscopy of molecules in the ISM, in particular, molecules embedded in the interstellar and circumstellar frozen material, the interstellar ice.

The ISM contains simple molecules such as CH, CO, and H_2, but also larger and more complex organic molecules (COMs[1]) such as glycolaldehyde, the simplest sugar molecule (Hollis et al., 2000). Molecules that are highly unstable in terrestrial environments, such as the cyanopolyynes[2], are also identified in interstellar environments. Carbon-based molecules in which the atoms are connected to form cage-like structures, such as the buckminsterfullerene (C_{60}), also figure in the molecular inventory list. Furthermore, it is estimated that 10 - 20% of all the carbon in the ISM is locked in large carbon-based compounds, the polycyclic aromatic hydrocarbons (PAH, Tielens 2008). These molecules, which on Earth are associated with the combustion of materials such as coal, oil, and wood, are found across a diversity of environments in the ISM.

[1] Molecule containing a C-H bond and at least 6 atoms
[2] Organic molecules with the chemical formula HC_nN

Probing the chemical composition of our Solar System, taught us that the chemistry in space could be even more fascinating. Space missions aimed at exploring moons, planets, and comets, revealed that organic molecules are ubiquitous. The Rosetta Orbiter Spectrometer for Ion and Neutral Analysis (ROSINA) onboard the Rosetta spacecraft has probed *in-situ* the composition of the comet 67P/Churyumov-Gerasimenko. These measurements allowed the detection of organic molecules even more complex than the ones found in the ISM, such as the amino acid glycine and benzoic acid, and a range of sulfur-containing molecules, such as sulfur allotropes and salts (Altwegg et al., 2016, 2022; Hänni et al., 2022). In addition, the comparison of the organic molecular inventory in the comet 67P and young stars indicates that the cometary material preserves molecules formed at the early stages of star formation (Drozdovskaya et al., 2019). Thus, the comet composition reveals the ingredients that were merged to form planets and other solid bodies in our Solar System.

The presence of organic compounds outside Earth does not necessarily imply that larger biological molecules, such as proteins and nucleic acids, exist in extraterrestrial environments. Thus far, laboratory and theoretical works simulating space environments have demonstrated that small organic species are important starting points to form these biological molecules, which are needed for life as we know to flourish (e.g., Meinert et al. 2016; Ligterink et al. 2018; Oba et al. 2019). Observing and studying the molecular diversity in space helps us to understand where and how these molecules are formed, and how they are spread in the cosmos. In the end, molecules can teach us about the origins of the Milky Way, our Solar System, and even ourselves.

1.1 Molecules in the stellar life cycle

The surreal beauty of astronomical pictures can give us the impression that the space between the stars, the ISM, is steady and quiet. This view of a calm place is challenged by the harsh conditions found in the ISM, where different environments experience extremes of temperature, ranging from 3 K to 10^5 K. Stars produce ionizing radiation and stellar winds during their life. Massive stars ($m > 8$ $M_\odot$) at the end of their lives explode as supernovae, heating their surroundings to very high temperatures ($T > 10^4$ K) and producing highly energetic particles (i.e., cosmic rays). These high-mass stars will potentially form a neutron star or black hole, which likely contains an accretion disk, that produces highly energetic radiation and particles. Under these hostile conditions and the generally low pressures found in the ISM (which limit collisions of atoms and molecules), it can be surprising that molecules form and any sort

of complex chemistry can flourish.

Molecular clouds are the key to this apparent puzzle. Molecular clouds are large and dense extensions of gas and dust formed by the gravitational collapse of the diffuse ISM material, as shown schematically in Figure 1.1 (indicated by the numbers I and II). The outer parts of a molecular cloud are composed of atomic gas and, in general, simple molecules (Snow and McCall, 2006). In these environments, the lifetime of molecules is relatively short, as ionizing radiation from stars and other sources can dissociate them. Deeper into the cloud, the radiation field is attenuated, as the cloud material shields itself, preventing photons and some particles to reach the cloud's densest parts (Draine, 2010). In such environments, larger molecules can form and survive for long periods.

In the denser parts of a molecular cloud ($\geq 10^4$ cm^{-3}) the gas is mostly molecular, and H_2 and CO are the most abundant species. In these regions, gas-phase formation of a few larger species is possible but these reaction routes generally do not account for the observed abundance of simple species, like water (H_2O), as well as COMs. The reasons for this are associated with the prevalence of two body processes in these environments, low collision rates, and the short time scale of the interaction in the gas phase. Under these conditions, the formation and observed abundances of COMs can only be accounted for by considering chemical reactions occurring on the surface of interstellar dust. Interstellar dust grains are agglomerates of silicates, carbonaceous material, and other minor elements (Draine, 2003) and represent on average 1% of the molecular cloud mass. At the cold temperatures found in the cloud's inner parts ($\sim$ 10 K), molecules and atoms accrete to the surface of these dust grains and form layers of frozen material, the so-called interstellar ice. At these surfaces, atoms can diffuse and react with other atomic or molecular species (Tielens and Hagen, 1982; Linnartz et al., 2015). Thus, these icy dust grains provide a place where interstellar chemistry can occur. Additionally, these grains act as a third body, where the energy released from chemical reactions can be dissipated, stabilizing the reaction products. Further chemical reactions may be triggered by UV photons, energetically charged particles, or the increase in the ice temperature. The research field that experimentally investigates these processes is known as solid-state astrochemistry

With the onset of star formation, the interstellar ice layers will pass through a sequence of physical and chemical transformations. As material falls onto the central forming star, its surroundings are heated (shown in III of Figure 1.1). This eventually causes the interstellar ice layers to sublimate. Once in the gas phase, these molecules can be probed through their rotational transitions at radio or submillimeter frequencies

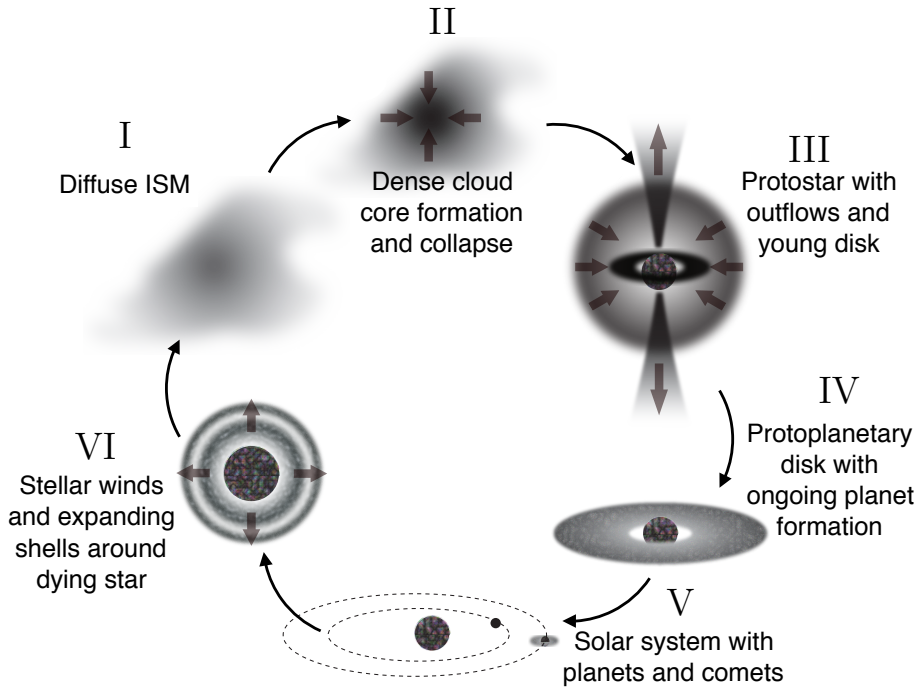

Figure 1.1: Schematic representation of the stellar life cycle. Star formation begins with the diffuse ISM (indicated in I), due to internal and external effects the diffuse ISM can start to collapse forming molecular clouds, and the densest regions of the molecular clouds start to form dense cores (II). The dense cores will collapse and form a protostar (III). As material falls onto the central protostar, a disk is formed, its surrounding is heated, and the protostar produces outflows of gas. After the star is formed a protoplanetary disk remains (IV) and forms planets and comets within $1 - 10$ Myrs (V). At the end of the life of the star (VI) it produces winds or explodes as a supernova bringing the elements produced in the stellar interior by nuclear fusion back to the diffuse ISM where the cycle of the star formation can repeat (based on Öberg, 2016).

(typically below 2 THz). Indeed, a diversity of molecules, including a remarkably large number of organic species have been observed in the warm ($T \sim 100$ K) and dense ($\geq 10^6$ cm^{-3}) gas surrounding high- and low-mass protostars by surveys performed with the Aratama Large Millimeter/submillimeter Array (ALMA, e.g., Jørgensen et al. 2020; van Gelder et al. 2020; Yang et al. 2021). Systematic studies of the warm gas around protostars indicate that the organic molecular inventory of these objects is set at the early stages of cloud evolution (Nazari et al., 2022). At these (pre-stellar) stages, the gas is almost completely frozen onto the dust grains (Caselli et al., 2022). Thus,

interstellar ice is considered the main source of organic molecules in the interstellar medium.

Part of the interstellar grains surrounding the newly formed stellar object will be incorporated into a rotating disk of gas and solid material, the protoplanetary disc (shown in IV of Figure 1.1). There, the interstellar grains will coagulate and form larger solid agglomerates, which will eventually form rocky bodies such as comets, moons, and planets. If the icy material coating the dust grains survives the collapse and the accretion process, the frozen molecular inventory can be incorporated into these bodies of the planetary system (V of Figure 1.1). The extent at which the frozen molecules created in the parent cloud are transferred onto the larger bodies is still uncertain. However, comparisons of the composition of the comet 67P, measured *in-situ* by the Rosetta mission, and solar-type young stars hint at the idea that cometary material is inherited from pre-stellar and protostellar stages (Drozdovskaya et al., 2019).

The stellar life cycle ends after many evolutionary stages. At its final stage (indicated by VI in Figure 1.1), the star produces winds that blow the circumstellar gas into the ISM. The most massive stars explode as supernovae, expelling the circumstellar gas and the heavier elements (e.g. C, N, O, S, Fe, Ni) that were produced through nuclear fusion (Carroll and Ostlie, 2017). All these processes enrich the gas from which a new generation of stars will be formed.

1.2 Interstellar ice

The existence of interstellar dust and its physical properties (e.g., composition, size, extinction) is debated since the 30's. The idea that H_2O and other molecules could stick to interstellar solid particles, coating them with a layer of frozen material, came later (van de Hulst, 1946). The first observational evidence for the existence of solid interstellar material came with the observation of silicate features around the 70's (Knacke et al., 1969; Woolf and Ney, 1969). In the years to come, absorption features of silicates, such as the 9.7 μm (Si-O stretching) and 18 μm (O-Si-O bending) bands, have been observed in absorption and emission toward several objects (e.g., Min et al. 2007; Draine 2003). The unambiguous detection of icy molecules happened in 1973 when the 3.1 μm absorption feature of H_2O ice was convincingly identified toward the Orion BN/KL region (Gillett and Forrest, 1973). In the decades that followed, other broad interstellar absorption bands were observed toward different infrared (IR) sources, which allowed for the identification of other solid-state species, such as CO

and CO_2, and the absorption of molecular functional groups whose carriers could not be fully identified, such as -CH_3 and -C=O (e.g., Soifer et al. 1979; Hagen et al. 1980; Lacy et al. 1984; d'Hendecourt and Jourdain de Muizon 1989; Grim et al. 1991; Lacy et al. 1991).

From 1995 onward, infrared observations using the Very Large Telescope (VLT), the Infrared Space Observatory (ISO), and the *Spitzer* Space Telescope, allowed for observing ice features at much higher resolution and sensitivity, and in the case of ISO and Spitzer, unhindered by the Earth's atmosphere. Several observing programs performed with these and other infrared facilities allowed for tracing the median molecular inventory of ices in different environments, as shown schematically in Figure 1.2 (which also includes abundances obtained by new JWST observations). Figure 1.2 shows that the composition of interstellar ice is dominated by water (H_2O). Carbon dioxide (CO_2) and carbon monoxide (CO) are also abundant, with abundances ranging from a few percent up to $\sim 50\%$ of the H_2O budget. The large variation observed for these molecules is due to the high variation in local conditions, such as dust temperature and radiation field (Boogert et al. 2015 and references therein). Also, methanol (CH_3OH) has been identified at abundances of a few percent up to $\sim 30\%$ with respect to solid H_2O. Ammonia (NH_3) and methane (CH_4) are detected as minor components, with relative abundances of $\leq 10\%$ with respect to solid H_2O. Less abundant species that were also identified are ^{13}CO, $^{13}CO_2$, OCN^-, and OCS. In addition to these molecules, H_2CO, HCOOH, and SO_2 are likely identified but stronger observational evidence is needed for definite assignments.

The James Webb Space Telescope (JWST), launched on the 25th of December of 2021, is capable of performing observations in the 0.6 - 28 μm range with high resolution and sensitivity. These observations will extend our understanding of inter- and circumstellar ices and their link to observed gas phase molecular abundances. At the moment of writing, the first ice observations with the JWST across the mid-infrared range have been made public (Yang et al., 2022; McClure et al., 2023). Figure 1.3 shows the 2.5 - 20 μm spectra of ices at dense parts (visual extinction, A_v, higher than 50) of the Chamaeleon I low-mass star-forming region. These observations show the densest quiescent cloud regions in which interstellar ice has been detected. The absorption bands of frozen molecules identified in these JWST observations are marked in different colors. Many known interstellar species are identified at these lines of sight, and some of them, such as CH_4, $^{13}CO_2$, and ^{13}CO, are detected toward regions illuminated by a background star for the first time. Section 1.2.3 describes in more detail how JWST will further our understanding of the interstellar ice composition.

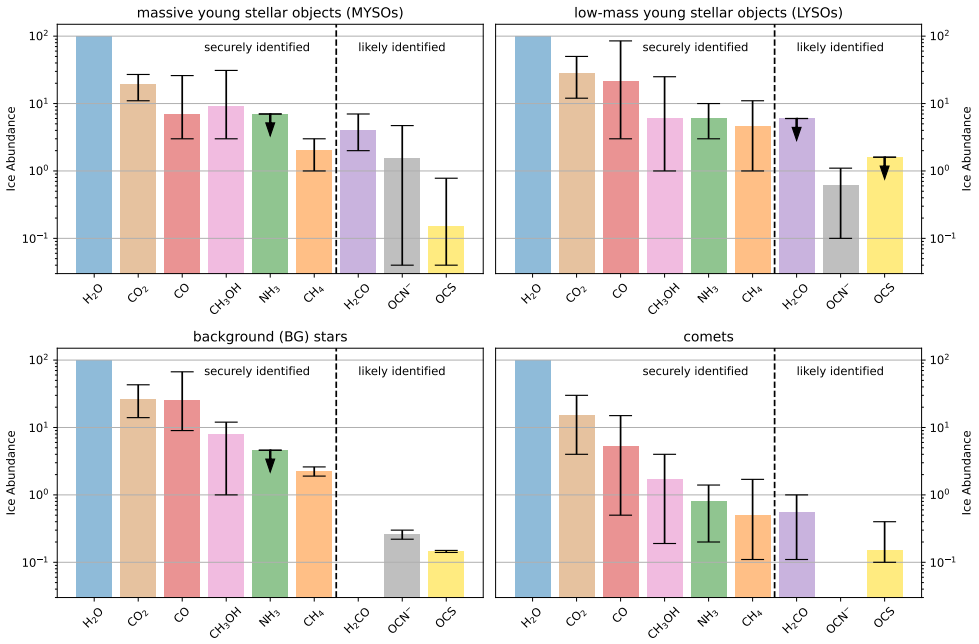

Figure 1.2: Relative abundance with respect to water (H_2O) for the nine most abundant icy molecules detected (or likely detected) towards massive young stellar objects (MYSOs; top left), low-mass young stellar objects (LYSOs; top right), background stars (BG, bottom left) and comets (bottom right). The black bars indicate the minimum and maximum detected values and the arrows indicate upper limits. The relative abundance values for MYSOs are from Boogert et al. 2015 for CO_2, CO, CH_3OH, NH_3, CH_4, and H_2CO, and from Boogert et al. 2022 for OCN^- and OCS. For LYSOs, all values are sourced from the compilation in Boogert et al. 2022. As for BG stars, the values for CO_2, CO, and CH_3OH are from Boogert et al. 2015, while the values for NH_3, CH_4, OCN^-, and OCS are obtained from McClure et al. 2023. For comets, the values for CO_2, NH_3, and H_2CO are from Mumma and Charnley (2011), the values for CH_3OH, CH_4, and CO, are taken from DiSanti and Mumma 2008 and for OCS from Saki et al. 2020.

1.2.1 The formation and evolution of interstellar ices

The identification of interstellar ice molecules has been largely based on accurate laboratory data, as available today from several databases, including LIDA, the Leiden Ice Database for Astrochemistry (Rocha et al., 2022). Spectroscopy works focusing on characterizing molecules under interstellar conditions are essential to determine the composition and morphology of interstellar ice as well as outline its evolutionary history. In the following, the current model for the formation and chemical evolution

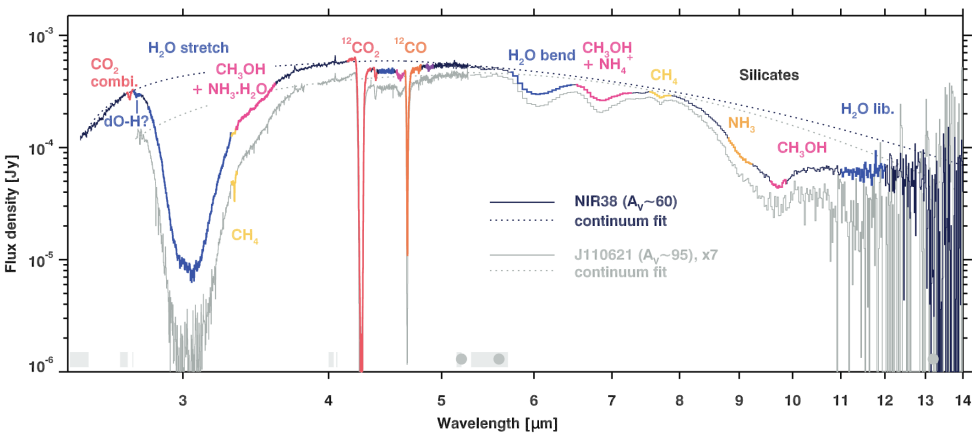

Figure 1.3: Mid-infrared spectrum of ices at dense ($A_v \geq 50$) regions of the Chamaeleon I region taken with JWST (from McClure et al. accepted). Marked in a different color are the different infrared molecular features identified in these ices. These lines of sight probe the interstellar frozen material in quiescent cloud regions, outside of the infalling envelope of a young stellar object (YSO).

of interstellar ice is shortly presented.

Figure 1.4 shows a schematic picture of different phases of ice formation and processing during the molecular cloud life stages. The formation of H_2O ice (indicated in I) starts in translucent clouds, which are regions of relatively low density ($A_v \sim 2$) in the cloud edges or early in the cloud evolution (van Dishoeck and Black, 1986; Whittet et al., 2001; Boogert et al., 2015). Under these conditions, the external ionizing and dissociating radiation are partially shielded, and the formation of icy molecules proceeds faster than their photodesorption, favoring interstellar ice growth. As a consequence, the condensation of hydrogen and oxygen atoms on the dust surfaces results in the formation of solid H_2O (Tielens and Hagen, 1982; Miyauchi et al., 2008; Ioppolo et al., 2008). At the same stage, the accretion of other atomic species is expected to lead to the formation of NH_3 and CH_4 via hydrogenation of nitrogen and carbon, respectively (Fedoseev et al., 2015; Qasim et al., 2020). In addition, the reaction of adsorbed CO molecules with OH leads to the formation of CO_2 (Ioppolo et al., 2011). In this phase, H_2O is the most abundant species, followed by CO_2. The ice formed at this phase is commonly referred to as 'polar ice' due to the high abundance of H_2O.

Deeper into the cloud or at later stages of the cloud evolution, the density increases, and gas-phase reactions lead to higher amounts of CO. Due to the low temperatures ($T \leq 20$ K), part of the CO accretes onto the dust grains. Thus, the formed frozen

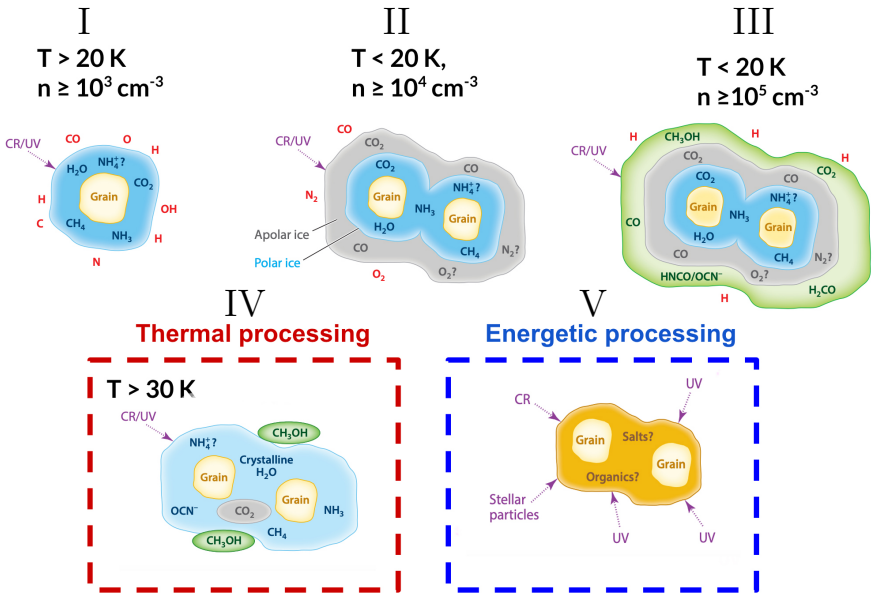

Figure 1.4: Schematic view of the evolution of interstellar ice and its different phases (adapted from Boogert et al., 2015). In phase I, H_2O is the most abundant species formed onto the dust grains, thus, this phase is known as polar ice. In this stage, NH_3, CH_4, and CO_2 are also formed. In phase II, CO is adsorbed, forming a layer of CO with less abundant volatiles, such as N_2 and O_2. The ice at this stage is known as apolar ice. Phase III is called the "catastrophic CO freeze-out" and is marked by increasing CO accretion. The hydrogenated CO leads to the formation of CH_3OH and H_2CO. With the onset of star formation, temperature increase causes desorption of more volatile species and segregation, as shown in IV. Phase V shows the energetic processing of the interstellar ice by UV and cosmic rays, causing chemical and morphological changes. These energetic agents can also process the ice material formed at early stages, inducing morphological changes in the ice and the formation of new molecules (Öberg, 2016).

material is rich in CO and is known as "apolar ice" (shown in II). At even later stages of the molecular cloud evolution, the gas density further increases ($n \geq 10^5$ cm^{-3}), the temperature drops, and consequently the accretion of CO and other volatile species is enhanced. This is phase is shown in III and is known as the 'catastrophic CO freeze-out'. The composition of the interstellar ice formed under such conditions is marked by abundant CO ice (Pontoppidan, 2006), CO_2 and the presence of more complex molecules, particularly the ones originating from the hydrogenation of CO, such as CH_3OH and H_2CO (Pontoppidan et al., 2004; Cuppen et al., 2009). In addition, laboratory work has shown that a variety of other COMs are formed in the hydrogenation network of CO, such as glycolaldehyde, methoxymethanol (H_3COCH_2OH),

and glyoxal (HC(O)CHO, see for example Linnartz et al. 2015; He et al. 2022b).

The onset of star formation leads to further transformations of the composition and morphology of the interstellar icy material (shown in IV). When the temperature increases above 20 K, the more volatile species sublimate. Thus, CO and other possibly present species, such as N_2 and O_2, desorb. In addition, recent laboratory investigation of solid CO indicates that changes in the ice structure below 20 K can induce migration of species buried within the ice, triggering chemical reactions (He et al., 2021, 2022a). Thus, the morphological transformation of CO ice at the early stages of star formation would significantly impact the chemical composition of the interstellar solid material. In this line, a laboratory investigation of structural changes in thick CO ice layers is studied in Chapter 5.

When the interstellar ice temperature rises from 30 K to 80 K, the sublimation of other species takes place. During this process, CO_2 molecules gain mobility and tend to agglomerate, forming domains of pure solid CO_2 within the ice (see IV in Figure 1.4). This process, known as segregation, can be probed by the infrared absorption profile of the CO_2 bending mode, at 15.2 μm (Ehrenfreund et al., 1998). Observing interstellar ice toward lines of sight probing warmer ices, one finds that the 15.2 μm band has a profile that is similar to the band in pure CO_2 (Pontoppidan et al., 2008). However, in lines of sight passing through regions where the ice temperature is below 20 K, the profile of the 15.2 μm is similar to those observed in mixtures with H_2O, CO, and CH_3OH, indicating that CO_2 is closely mixed with these molecules (Ehrenfreund et al., 1998; Pontoppidan et al., 2008). In addition to segregation, the increase in ice temperature can cause the crystallization of water ($T \geq 80$ K) and the formation of more complex organic species through thermal reactions (Theulé et al., 2013).

The energetic processing of interstellar ice (shown in V) by ultraviolet radiation and energetic particles causes several chemical and morphological changes in the ice material. Over the years, a vast amount of experimental works simulated the energetic processing of interstellar ices analogs, showing that these can induce the formation and destruction of frozen species (Munoz Caro et al., 2002; Gerakines et al., 1995; Rothard et al., 2017), photodesorption (Öberg et al., 2007; Bertin et al., 2016; Muñoz Caro et al., 2016) and sputtering (by particles; Dartois et al., 2019) of icy molecules, and morphological changes in the ice structure, as compaction and amorphization (Raut et al., 2007; Dartois et al., 2015). Besides the similarities between the IR profile of interstellar ice and the irradiated laboratory ice analogs, the extent to which energetic processes shape the composition and morphology of the interstellar solid material remains undetermined (Boogert et al., 2015).

1.2.2 COMs in interstellar ices

The high complexity of interstellar molecules detected in the gas phase (Herbst and van Dishoeck, 2009; Belloche et al., 2013; Jørgensen et al., 2016) contrasts with the ice inventory shown in Figure 1.2. In fact, most of the COMs detected in the gas are expected to form in the ice phase (Garrod et al., 2022) and transfer to the gas through different mechanisms, such as thermal-induced sublimation, photodesorption, sputtering, and reactive desorption (Minissale et al., 2022, and references therein). The difficulty in unambiguously detecting frozen COMs has several reasons, among which: i) the low abundances of COMs in ice, which is estimated as a few percent; ii) the overlap of the absorption features of molecules with similar structural characteristics; and iii) the sensitivity and resolution of past interstellar ice surveys, that did not allow to detect and resolve weak COM features, that usually correspond to absorption of a few percent of the continuum level.

Although not conclusive, weak absorption features in the mid-infrared spectrum of protostars have been tentatively associated with COMs, as shown in Figure 1.5. Observations of high-mass YSOs with ISO and low-mass YSO with Spitzer show absorption features at 7.41 and 7.24 μm, which have been tentatively assigned to organic species, such as HCOOH, CH_3CHO, and CH_3CH_2OH (Schutte et al., 1999; Boogert et al., 2011). Some of these tentative defections have been revisited in other works (Öberg et al., 2011; Terwisscha van Scheltinga et al., 2018) but no final assignment was possible. A better agreement with the position and width of these molecule's features in relevant astronomical ices is needed, something that has not been possible due to the blend of features and, in the case of observations performed with Spitzer, low spectral resolving power (R $\sim$ 100). In addition, a decisive assignment of these features would require the detection of other absorption bands assigned to their carriers.

1.2.3 Looking to the future: interstellar ices in the JWST era

JWST is equipped with four instruments, the Near-Infrared Camera (NIRCam), the Near-Infrared Spectrograph (NIRSpec), the Mid-Infrared Instrument (MIRI), and the Fine Guidance Sensor/Near InfraRed Imager and Slitless Spectrograph (FGS/NIRISS), that together cover the range from 0.6 - 28 μm. Combined observations using the NirSpec and MIRI instruments will allow for scanning the ice absorption signatures throughout the whole mid-infrared range. In particular, observations with the MIRI Medium Resolution Spectrometer (MIRI/MRS) allow for the detection of ice features in the 5.3 - 28 μm range with resolving power $\Delta\lambda/\lambda \sim 3000$. This includes the fin-

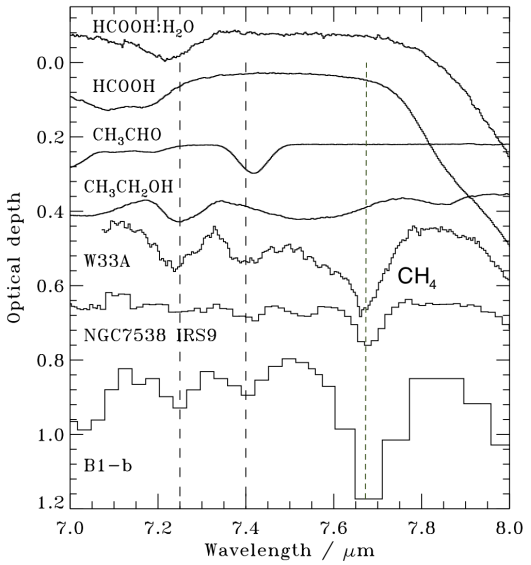

Figure 1.5: Comparison between the ISO spectra of the high-mass YSOs W33 A and NGC 7538 IRS 9, the Spitzer spectrum of the low-mass YSO B1-b and laboratory ice spectra of HCOOH, CH_3CHO, and CH_3CH_2COH (from Öberg et al., 2011). The 7.24, 7.41, and 7.67 μm features are marked with a vertical dashed line.

gerprint region between $\sim$ 6.5 - 20 μm, which is the most suitable spectral window to identify characteristic absorption features of many molecules, including COMs.

Recent observations of interstellar ice with the JWST are already bringing new insights into the composition of the interstellar solid material. Currently, observations of interstellar ice performed within two JWST observation programs have been made public. These are the Early Release Program 'Ice Age' (ID 1309, McClure et al., 2017; McClure et al., 2023) and the General Observer program 'Blazing the trail of COMs from ice to gas' (ID 2151, Yang et al., 2021), here 'Corinos I' (Yang et al., 2022). As previously mentioned, the results of the Ice Age program allowed for a view of ices in dense regions of a molecular cloud ($A_v \geq 50$). Observations with the low-resolution mode of MIRI indicate the presence of COM features, that are tentatively assigned to acetone (CH_3COCH_3), ethanol, and acetaldehyde (CH_3CHO). McClure et al. suggested that these lines of sight should be observed with the MIRI MRS to confirm the identifications.

The observation from the Corinos I revealed a richness of details in the MIRI-MRS spectrum of ices toward a low-mass young stellar object. In the observed spectrum, the 7.41 and 7.24 μm features associated with COMs and absorption features

at 5.83 and 6.7 μm, associated with H_2CO, are seen at much higher resolution. This result is a glimpse into the potential of MIRI-MRS to resolve weak spectral signatures of COMs. In 2023 and the following years, observations of ice at different stages of star formation are envisioned within the Ice Age, the MIRI GTO program JOYS, and other JWST observation programs. This will shed light on the formation history of ices and help to understand when and how organic molecules are formed in the stellar life cycle.

1.3 Laboratory astrophysics: spectroscopy

Laboratory astrophysics consists of experimental and theoretical studies as well as computational modeling of the chemistry in extraterrestrial environments. In other words, this research domain focuses on the chemistry between the stars, dealing with the chemical reactions and spectroscopy of atoms and molecules in simulated astronomical conditions. By performing investigations under fully controlled conditions, the properties and chemical evolution of matter in space can be understood. In this thesis, the focus is on the experimental spectroscopy of molecules in the solid state, with special attention on COMs. The recorded spectra of frozen molecules allow for interpreting interstellar ice observations, linking the interstellar solid and gas-phase molecular inventory, and providing input to astrochemical models. The following sections outline general aspects of vibrational spectroscopy, the tool to identify ices in space, and the laboratory work aimed at supporting astronomical observations, especially the ones performed with JWST.

1.3.1 Vibrational spectroscopy

The interaction of molecules and electromagnetic radiation is ruled by the quantization of energy, the ground principle of quantum mechanics. According to these rules, the energy carried by electromagnetic radiation can be transferred to or from molecules only in very specific amounts, which correspond to the difference between two molecular energy levels. Molecular spectroscopy is the study of the absorption and emission of light based on the involved molecular energy levels.

The absorption of light in different domains of the electromagnetic spectrum induces different transitions within a molecule. The absorption of light in the ultraviolet and visible wavelengths excites electrons to different levels of energy. Light in the infrared domain induces molecular vibrations, and radiation in the microwave and at radio wavelengths induces molecular rotations and transitions of the hyperfine struc-

ture of matter. In the following, some characteristics of vibrational spectroscopy and their importance to interstellar ice observations are presented.

The absorption of infrared light at resonant wavelengths can induce molecular vibrations. To absorb or emit radiation, the molecular vibration must give origin to a non-zero dipole moment derivate, $d\mu/dR \neq 0$ with R the distance between atoms, and the frequency of the radiation and the vibrating dipole has to be the same. This brings us to one important point: isolated homonuclear diatomic molecules (e.g., H_2, O_2, N_2) do not have dipole-allowed transitions. Because the electronegativity of the vibrating atoms is the same, $d\mu/dR$ is zero. However, laboratory experiments have shown that when O_2 is immersed in certain environments (i.e., ice matrices), the absorption of infrared light can be induced (Ehrenfreund et al., 1992; Müller et al., 2018), which leads to an important point about vibrational spectroscopy: *molecular vibrations and thus the infrared absorption profile of a molecule are influenced by its surroundings.*

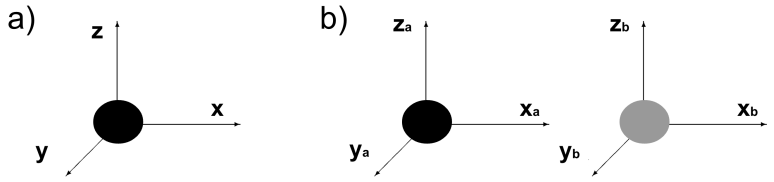

Figure 1.6: Degrees of freedom of a single particle (a), and a two-particle system (b).

Diatomic molecules are simple systems to study molecular motions, as their vibration can just occur in the axis of the molecular bond. The vibrational motions of polyatomic molecules are more complex. The atomic motions within a molecule can be understood and modeled in terms of a limited number of fundamental motions, the so-called normal modes of vibrations. This is schematically visualized in Figure 1.6. The movement of a single particle in space can be fully decomposed into motions along three orthogonal directions, here x, y, and z. Thus, this particle has three degrees of freedom. Consider now a system composed of two particles (e.g., two nuclei of a diatomic molecule). This system has six degrees of freedom. Any motion of the particle can be decomposed into motions along these six coordinates. Three of these degrees of freedom are translation motions of the molecule as a whole (when both particles move in the same direction), two are rotations about the center of mass, and one is the undefined rotation about the molecular axis (which is only defined for non-linear molecules). All the movements of a molecule can be decomposed in terms of these individual motions. This has the consequence that the number of vibrations

of a non-linear molecule with n atoms is given by N = $3n$ - 6, while the number of vibrations for a linear molecule is given by N = $3n$ - 5 (as a rotation around the molecular axis does not lead to any change). As previously mentioned, not all the possible vibrational motions of a molecule will result in the absorption of IR light, just the ones with a non-zero change in the dipole moment. In addition, some vibrational motions have the same energy, the so-called degenerate modes. Thus, the number of observable vibrational bands can slightly differ from the predicted.

In general, specific transitions between vibrational levels of a molecule occur within certain infrared domains and compose the molecular fingerprint. The transition of a combination of fundamental vibrational modes and overtones (transitions from the ground state of a molecule to the second or higher excited states) typically occurs in the near-infrared, around the 1 - 3 μm region. Stretching vibrations of chemical bonds absorb light between 3 - 6 μm. Bending motions and librations occur in the 6 - 30 μm region. Torsional and lattice modes occur in the far-infrared 30 - 300 μm. Since the vibrational spectrum of a molecule is determined by the combined motion of its atoms, the absorption profile of molecules with similar substructures shows commonalities. A group of atoms connected in a specific way causing the molecule to undergo specific chemical reactions is called a functional group. Examples of functional groups are the carbonyl, where the carbon and oxygen are linked by a double bond (C=O), the hydroxyl (O-H), and the primary amine (-NH_2). The vibrational motions of functional groups within molecules give rise to vibrations at similar wavelengths. In solids and liquids, the various chemical environments of a molecule and the intermolecular interactions result in broad absorption bands. This brings another important characteristic of vibrational spectroscopy: *while this is a powerful technique to obtain information about the molecular structure, distinguishing molecules with similar structure in solid and liquid mixtures is challenging.* Figure 1.7 shows examples of the absorption profiles of the following pure ices at 15 K: H_2O, CH_3OH, formic acid (HCOOH), H_2CO, acetone (C_3H_6O), and methylamine (CH_3NH_2). The yellow-shaded areas show typical frequency regions where a few vibrations occur, namely the O-H, N-H, and C-H stretching and the C=O stretching. In addition, the fingerprint region is indicated with a shaded gray area. In this region, bending modes and other absorption of vibrations that are unique to each molecular structure occur. Figure 1.7 evidences the overlap in the absorption features of molecules containing similar structures. Examples of such overlap are the -OH stretching vibration of CH_3OH and H_2O, the C=O stretching of formic acid, formaldehyde, and acetone, and the C-H stretching of all the organic molecules displayed in the figure.

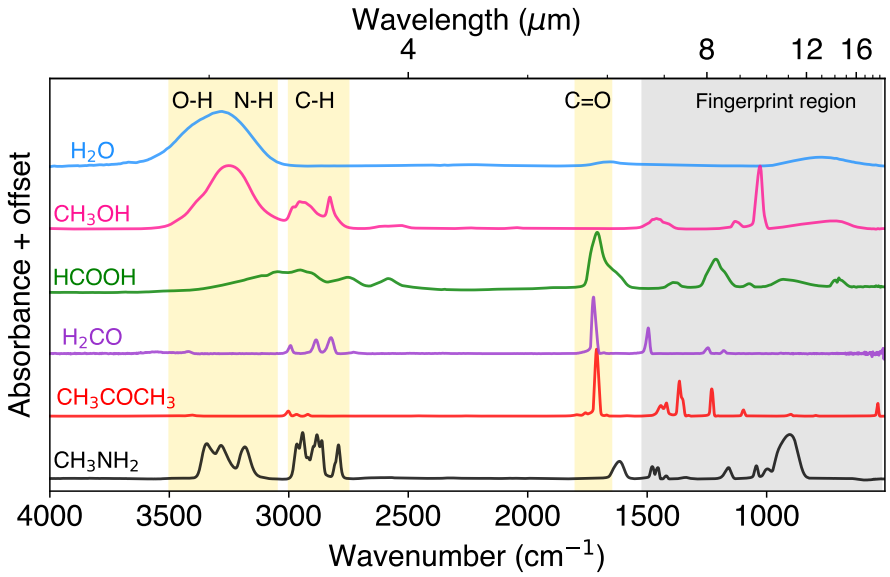

Figure 1.7: Normalized mid-infrared spectra of H_2O, CH_3OH, formic acid (HCOOH), H_2CO, acetone (C_3H_6O), and methylamine (CH_3NH_2). The shaded yellow areas indicate the typical frequency regions where a few stretching vibrations occur. The fingerprint region, indicated by the gray shaded area, is where the bending modes and other unique vibration modes absorb. This regions is the most useful to detect organic molecules in interstellar ice observations.

1.3.2 Spectroscopy of interstellar ice analogs

The absorption profile of a molecule is sensitive to the ice temperature, interaction with neighbor species (e.g., hydrogen bonding, dipole-dipole interactions), and ice morphology. The intermolecular interactions alter the electronic density within a molecule, consequently changing the frequency at which a molecular fragment vibrates. Also, the co-existence of different arrangements of a species within the ice structure causes absorption of light at slightly different wavelengths, which produces a broadening of absorption bands. In addition, molecular vibrations originating from molecules with similar structures overlap. In interstellar ice, this results in an absorption profile that is not trivial to disentangle. Laboratory measurements of frozen molecules under interstellar conditions are aimed at characterizing these effects, providing suitable spectroscopic data to compare to astronomical observation. To disentangle the overlap of infrared bands, algorithms that use laboratory spectra to decompose the interstel-

lar ice profile have been developed (Rocha et al., 2021). Still, the carriers of several observed interstellar ice features remain unassigned.

In addition to the ice environment effects, the absorption profile of frozen molecules changes with the shape and size distribution of interstellar grains in space. This is usually observed for major ice components, such as H_2O, CO_2, and CO (Baratta et al., 2000; Pontoppidan et al., 2003; Dartois et al., 2022). Furthermore, the features of the dust material also contribute to the absorption profile in the mid-infrared (Krügel and Siebenmorgen, 1994; Henning, 2010). Thus, in a more complete analysis, the interstellar ice profile in the infrared is only fully accounted for when the absorption and scattering of dust and icy material of specific geometry and size distributions are considered (Preibisch et al., 1993; Min et al., 2007; Dartois et al., 2022).

With the discovery of interstellar ice, back in the 70's, laboratory spectroscopic work at simulated astronomical conditions became essential. At the beginning of the 80's, the Laboratory for Astrophysics at the Leiden Observatory was pioneering in acquiring the spectra of solid samples in interstellar conditions (Hagen et al., 1980, 1981; Greenberg et al., 1983; d'Hendecourt and Allamandola, 1986) aiming at supporting infrared observations. Over the years, the spectroscopic research of ice analogs grew worldwide, especially stimulated by ISO (e.g., Gerakines et al. 1995; Ehrenfreund et al. 1997) allowing all the discoveries outlined in the previous sections. Nowadays, several laboratories perform extensive spectroscopic works aimed at interpreting astronomical data, and more recently supporting the observations obtained with the JWST (see for example Maté et al. 2017; Urso et al. 2017; Luna et al. 2018; Hudson and Gerakines 2018; Terwisscha van Scheltinga et al. 2018; Scirè et al. 2019; Palumbo et al. 2019; Hudson et al. 2021; Terwisscha van Scheltinga et al. 2021; Müller et al. 2022; Gerakines et al. 2022). Chapters 2, 3, and 4 (Rachid et al., 2020; Rachid et al., 2021; Rachid et al., 2022) of this thesis add to these efforts. In these works, the spectra of three frozen COMs (C_3H_6O, CH_3NH_2, and CH_3CN) under a range of interstellar relevant conditions (e.g., temperature, ice composition) are measured. The acquired laboratory data also allow for determining absorption cross-sections that can be used to constrain the abundance of these species in interstellar ice.

To simulate the effects that change the infrared profile of a molecule in the ISM, it is necessary to measure the spectra of samples in realistic astronomical conditions. The ISM regions where interstellar ices exist have gas densities of around 10^3 - 10^6 cm^{-3}, which is orders of magnitude below the conditions found in the Earth's atmosphere ($\sim 10^{19}$ cm^{-3}). Also, the temperatures in which interstellar ice can exist (T $\sim$ 10 - 150 K) require the use of experiments at cryogenic conditions. The experimental setups

used to record infrared spectra of frozen molecules at such conditions are described in detail in Chapter 2.

1.4 Calculation of the molecular vibrational profile

The laboratory methods and investigation described previously deal with the spectroscopy of molecules that are stable under terrestrial conditions. These molecules are easily purchased from chemical suppliers and introduced into experimental setups to perform spectroscopy measurements. In space, however, the different physical conditions allow for the existence of exotic molecules, that are unstable under terrestrial conditions. To study these species, several laboratory methods have been developed (Zack and Maier, 2014), as the *in-situ* generation of unstable species under inert conditions (Gudipati, 2004; Tsuge et al., 2018). Another approach is the use of computational molecular spectroscopy. These are a series of computational methods aimed at modeling the energy levels of a molecule using quantum mechanics (Barone et al., 2021). Shortly, the energy levels of atoms and molecules obey the Schrödinger equation:

$$H\Psi = E\Psi, \tag{1.1}$$

where Ψ is the wavefunction describing the molecule, H is the Hamiltonian operator, which describes the energy of the system, and E is the molecular energy level. Several methods have been developed to numerically solve this equation for molecular systems. One of the most popular methods to predict the electronic structure of large molecules is the density functional theory (DFT, Hohenberg and Kohn, 1964; Levy, 1979; Barone et al., 2015; Candian and Mackie, 2017). This method is based on describing a given system in terms of its electronic density (ρ(r)) as a function of space coordinates only, which simplifies the treatment of large molecules. In Chapter 7 (Candian et al., 2019), the vibrational spectra and insights on the stability of carbon cage molecules (i.e, fullerenes) are presented. The fullerenes C_{60} and C_{70} have been identified for the first time through their vibrational bands in the spectra of the protoplanetary nebula Tc 1 (Cami et al., 2010). Following this detection, fullerenes have been identified toward several objects at late stages of stellar evolution, in the ISM, and YSOs (Sellgren et al., 2010; Castellanos et al., 2014; Berné et al., 2017, and references therein). These discoveries raised speculations if other carbon-cage molecules are present in these environments. Since performing laboratory measurements with these species is challenging and still limited to a few species (Leidlmair et al., 2012; Maier

and Campbell, 2017), computational methods are essential to explore their properties and spectroscopy.

1.5 Thesis outline

This thesis seeks to investigate the spectroscopy of organic molecules in interstellar environments, focusing on the composition of interstellar ice. The ultimate goal is to shed light on the evolution of the chemical inventory throughout stellar evolution. With this purpose, Chapters 3, 4, and 5 present the mid-infrared spectroscopic characterization of three COMs (acetone, methylamine, and methyl cyanide) in different ice mixtures and give insights into their presence in interstellar ice. These molecules were identified in the gas phase in the ISM but their formation routes are expected to happen in interstellar ice. Furthermore, laboratory studies have shown that chemical reactions involving these molecules can give origin to more complex species in interstellar environments (e.g., Ioppolo et al. 2021; Bulak et al. 2021). The spectroscopic studies performed here help to address the questions: i) Can COMs be detected in JWST observations of interstellar ices?, and ii) What information about the ice composition can be derived from the IR spectral profile of these frozen molecules? Chapter 6 provides a systematic study of morphological changes taking place in CO ices using laser interference. Since CO is expected to be one of the main components of interstellar ice, its properties at different conditions will influence the chemistry and spectral profile of molecules mixed with it. Lastly, Chapter 7 is a computational study to predict the stability and the vibrational spectra of fullerenes containing 44 and 70 carbon atoms. More details about these works are summarized below:

- **Chapter 3** presents mid-infrared spectra of frozen CH_3COCH_3 in the pure form and mixed with H_2O, CO_2, CO, and CH_3OH. The spectra are acquired under high-vacuum (P $\sim 10^{-7}$ mbar) conditions and at cryogenic temperatures (T $\sim$ 15 - 160 K). The characterization of peak position and the full width of half maximum (FWHM) of bands that have the highest potential to be detected in upcoming JWST observation of interstellar ice is performed.
- **Chapter 4** uses the same experimental setup and methodology of Chapter 2 to characterize the mid-infrared spectra of frozen CH_3NH_2 in the pure form and mixed with H_2O, CH_4, and NH_3. In addition, this chapter presents upgrades performed to the previously used HV system. The new setup, IRASIS (InfRared Absorption Setup for Ice Spectroscopy) achieves achieve ultra-high-vacuum pressures and allows for measuring the refractive index of ices using

a laser interference technique. The refractive index measurements allowed for measuring ice thicknesses, which are combined with the infrared spectroscopy measurements to provide infrared band strengths of frozen methylamine. In this work, upper limits for the methylamine abundance in interstellar ice toward protostars are derived by comparing the laboratory spectra with observations. The observational data are archival data from Spitzer, Keck, VLT, and IRTF.

- **Chapter 5** presents mid-infrared spectra of frozen CH_3CN in the pure form and mixed with H_2O, CO_2, CO, CH_4, and NH_3, acquired with the IRASIS setup. The refractive index and band strengths of methyl cyanide at 15 K are also presented. The acquired spectroscopy measurements are compared to archival data from Spitzer and ISO, allowing for determining upper limits for CH_3CN in interstellar ice.
- **Chapter 6** uses interference techniques from ultraviolet to visible wavelengths (250 - 750 nm) to investigate morphological transitions in pure CO ice. In this work, μm-thick CO ices are grown under high vacuum conditions (P $\sim 10^{-8}$ mbar) at a temperature ranging from 7.5 - 18 K. After its growth, the ice is opaque and scatters incident light. After a certain time, morphological changes in the ice structure lead to a transparent ice. The aspects that influence the transition of opaque CO ice to transparent ice under various growing conditions, (i.e., deposition rate, temperature, and ice thickness) are analyzed. Insights into the ice structural changes taking place are also discussed.
- **Chapter 7** presents a computational study that uses DFT to investigate the infrared profile of neutral and singly ionized fullerene cages containing 44 up to 70 carbon atoms. The stability of these molecules is analyzed using the standard enthalpy of formation per CC bond, the HOMO–LUMO gap, and the energy required to eliminate a C_2 units. The obtained mid-infrared spectra of the cages were compared to the Spitzer spectra of fullerene-rich planetary nebulae.

1.6 Summary of main conclusions

The major conclusions of this thesis are summarized as follows:

I) Laboratory measurements of the infrared profile of organic molecules under astronomical relevant conditions are essential to interpret interstellar ice observations. Comparing observations with the laboratory spectra acquired under varying conditions allows for obtaining information about the interstellar ice conditions, such as temperature and the degree of mixing of icy molecules. Chapters 3, 4, and 5 present spectro-

scopic work to allow future searches of acetone, methylamine, and methyl cyanide in interstellar ice observations with JWST. From the spectral analysis of these molecules, the following conclusions are drawn:

- The features that show the most potential to identify acetone are a combination of the 5.85, 7.34, and 8.14 μm features.
- Methylamine absorption bands will be challenging to identify in interstellar ices due to significant overlap with H_2O and NH_3 features. With this caveat, the most promising features to identify this species in ice observations are the 3.45 μm and the 8.62 μm features. Using the 3.45 μm feature, the upper limits for methylamine abundance toward YSOs are estimated to be around $\leq$ 4 % with respect to solid H_2O.
- The features that show the most potential to identify methyl cyanide in interstellar ices are a combination of the 4.44 and the 9.60 μm features. Using these features, the methyl cyanide abundance toward YSOs is estimated as a few up to $\leq$ 4.1 % with respect to solid H_2O.

II) Structural transitions after the deposition of μm-thick CO ice can alter its scattering properties. Freshly deposited CO ice scatters visible light. After a certain time period, spontaneous morphology transitions lead to a transparent ice. The time scale for these transitions is dependent on the deposition temperature and thickness of the ice sample. The time scale for these transitions to happen ($\leq$ 1 year) is negligible compared to astronomical time scales but should be accounted for in laboratory experiments.

III) Neutral and singly charged fullerene cages consisting of 44 up to 70 carbon atoms have IR-active modes between 6 – 9 μm and can contribute to the emission profile observed toward the fullerene-rich planetary nebula. However, their vibrational spectra cannot simultaneously account for the 10 - 13 μm emission '*plateau*' observed in the same objects. The calculations show that the smaller fullerene cages show features in the 13 - 15 μm that resemble the emission features observed in LMC56 and SMC16.

References

Altwegg, K., Balsiger, H., Bar-Nun, A., et al., 2016, Science Advances, 2, e1600285
Altwegg, K., Combi, M., Fuselier, S. A., et al., 2022, MNRAS, 516, 3900
Baratta, G., Palumbo, M., and Strazzulla, G, 2000, A&A, 357, 1045

1.6. REFERENCES

Barone, V., Alessandrini, S., Biczysko, M., et al., 2021, Nature Reviews Methods Primers, 1, 1

Barone, V., Biczysko, M., and Puzzarini, C., 2015, Accounts of Chemical Research, 48, 1413

Belloche, A., Müller, H. S., Menten, K. M., et al., 2013, A&A, 559, A47

Berné, O, Cox, N., Mulas, G., et al., 2017, A&A, 605, L1

Bertin, M., Romanzin, C., Doronin, M., et al., 2016, ApJL, 817, L12

Boogert, A. C. A., Brewer, K., Brittain, A., et al., 2022, arXiv e-prints, arXiv:2210.12639

Boogert, A. C. A, Gerakines, P. A., and Whittet, D. C., 2015, ARA&A, 53, 541

Boogert, A. C. A., Huard, T. L., Cook, A. M., et al., 2011, ApJ, 729, 92

Bulak, M, Paardekooper, D., Fedoseev, G, et al., 2021, A&A, 647, A82

Cami, J., Bernard-Salas, J., Peeters, E., et al., 2010, Science, 329, 1180

Candian, A., Gomes Rachid, M., MacIsaac, H., et al., 2019, MNRAS, 485, 1137

Candian, A. and Mackie, C. J., 2017, International Journal of Quantum Chemistry, 117, 146

Carroll, B. W. and Ostlie, D. A. (2017). *An introduction to modern astrophysics*. Cambridge University Press.

Caselli, P., Pineda, J. E., Sipilä, O., et al., 2022, ApJ, 929, 13

Castellanos, P., Berné, O., Sheffer, Y., et al., 2014, ApJ, 794, 83

Cuppen, H. M., van Dishoeck, E. F., Herbst, E., et al., 2009, A&A, 508, 275

Dartois, E, Augé, B, Boduch, P, et al., 2015, A&A, 576, A125

Dartois, E, Chabot, M, Barkach, T. I., et al., 2019, A&A, 627, A55

Dartois, E., Noble, J. A., Ysard, N., et al., 2022, A&A, 666, A153

d'Hendecourt, L. and Allamandola, L., 1986, A&AS, 64, 453

d'Hendecourt, L. and Jourdain de Muizon, M, 1989, A&A, 223, L5

DiSanti, M. A. and Mumma, M. J., 2008, Space Science Reviews, 138, 127

van Dishoeck, E. F. and Black, J. H., 1986, ApJS, 62, 109

Draine, B. T., 2003, ARA&A, 41, 241

Draine, B. T. (2010). *Physics of the interstellar and intergalactic medium*. Vol. 19. Princeton University Press.

Drozdovskaya, M. N., van Dishoeck, E. F., Rubin, M., et al., 2019, MNRAS, 490, 50

Ehrenfreund, P., Boogert, A. C. A., Gerakines, P. A., et al., 1997, A&A, 328, 649

Ehrenfreund, P, Breukers, R, d'Hendecourt, L, et al., 1992, A&A, 260, 431

Ehrenfreund, P, Dartois, E, Demyk, K, et al., 1998, A&A, 339, L17

Fedoseev, G., Ioppolo, S., Zhao, D., et al., 2015, MNRAS, 446, 439

Garrod, R. T., Jin, M., Matis, K. A., et al., 2022, ApJS, 259, 1

van Gelder, M., Tabone, B., van Dishoeck, E., et al., 2020, A&A, 639, A87

Gerakines, P. A., Schutte, W. A., Greenberg, J. M., et al., 1995, A&A, 296, 810

Gerakines, P. A., Yarnall, Y. Y., and Hudson, R. L., 2022, MNRAS, 509, 3515

Gillett, F. C. and Forrest, W. J., 1973, ApJ, 179, 483

Greenberg, J. M., van de Bult, C., and Allamandola, L. J., 1983, The J. Phys. Chem., 87, 4243

Grim, R., Baas, F, Greenberg, J., et al., 1991, A&A, 243, 473

Gudipati, M. S., 2004, The J. Phys. Chem. A, 108, 4412

Hagen, W, Allamandola, L., and Greenberg, J., 1980, A&A, 86, L3

Hagen, W, Tielens, A., and Greenberg, J., 1981, Chem. Phys., 56, 367

Hänni, N., Altwegg, K., Combi, M., et al., 2022, Nat. communications, 13, 3639

He, J., Góbi, S., Ragupathy, G., et al., 2022, ApJL, 931, L1

He, J., Simons, M., Fedoseev, G., et al., 2022, A&A, 659, A65

He, J., Toriello, F. E., Emtiaz, S. M., et al., 2021, ApJL, 915, L23

Henning, T., 2010, ARA&A, 48, 0

Herbst, E. and van Dishoeck, E. F., 2009, ARA&A, 47, 427

Hohenberg, P. and Kohn, W., 1964, Phys. Rev., 136, 864

Hollis, J. M., Lovas, F. J., and Jewell, P. R., 2000, ApJ, 540, L107

Hudson, R. L. and Gerakines, P. A., 2018, ApJ, 867, 138

Hudson, R. L., Gerakines, P. A., Yarnall, Y. Y., et al., 2021, Icarus, 354, 114033

van de Hulst, H. C. (1946). "88. The Solid Particles of Interstellar Space". *A Source Book in A&A, 1900–1975*. Harvard University Press, 605.

Ioppolo, S., Cuppen, H. M., Romanzin, C., et al., 2008, ApJ, 686, 1474
Ioppolo, S., Fedoseev, G., Chuang, K. J., et al., 2021, Nat. Astronomy, 5, 197
Ioppolo, S., van Boheemen, Y., Cuppen, H. M., et al., 2011, MNRAS, 413, 2281
Jørgensen, J. K., Belloche, A., and Garrod, R. T., 2020, ARA&A, 58, 727
Jørgensen, J., Wiel, M. Van der, Coutens, A, et al., 2016, A&A, 595, A117
Knacke, R. F., Gaustad, J. E., Gillett, F. C., et al., 1969, ApJL, 155, L189
Krügel, E and Siebenmorgen, R, 1994, A&A, 288, 929
Lacy, J., Baas, F, Allamandola, L., et al., 1984, ApJ, 276, 533
Lacy, J., Carr, J., Evans, N. J., et al., 1991, ApJ, 376, 556
Leidlmair, C., Wang, Y., Bartl, P., et al., 2012, Phys. Rev. Letters, 108, 076101
Levy, M., 1979, Proceedings of the National Academy of Science, 76, 6062
Ligterink, N., Terwisscha van Scheltinga, J, Taquet, V, et al., 2018, MNRAS, 480, 3628
Linnartz, H., Ioppolo, S., and Fedoseev, G., 2015, Int. Rev. Phys. Chem., 34, 205
Luna, R., Molpeceres, G., Ortigoso, J., et al., 2018, A&A, 617, A116
Maier, J. P. and Campbell, E. K., 2017, Angewandte Chemie International Edition, 56, 4920
Maté, B., Molpeceres, G., Timón, V., et al., 2017, MNRAS, 470, 4222
McClure, M. K., Rocha, W. R. M., Pontoppidan, K. M., et al., 2023, Nat. Astronomy,
McClure, M., Bailey, J., Beck, T., et al. (Nov. 2017). *IceAge: Chemical Evolution of Ices during Star Formation*. JWST Proposal ID 1309. Cycle 0 Early Release Science.
McGuire, B. A., 2022, ApJS, 259, 30
Meinert, C., Myrgorodska, I., De Marcellus, P., et al., 2016, Science, 352, 208
Min, M, Waters, L., Koter, A. de, et al., 2007, A&A, 462, 667
Minissale, M., Aikawa, Y., Bergin, E., et al., 2022, ACS Earth and Space Chemistry, 6, 597
Miyauchi, N., Hidaka, H., Chigai, T., et al., 2008, Chem. Phys. Lett., 456, 27
Muñoz Caro, G. M., Chen, Y. J., Aparicio, S., et al., 2016, A&A, 589, A19
Müller, B., Giuliano, B. M., Vasyunin, A., et al., 2022, A&A, 668, A46
Müller, B, Giuliano, B., Bizzocchi, L, et al., 2018, A&A, 620, A46
Mumma, M. J. and Charnley, S. B., 2011, ARA&A, 49, 471
Munoz Caro, G., Meierhenrich, U. J., Schutte, W. A., et al., 2002, Nat., 416, 403
Nazari, P., Meijerhof, J. D., van Gelder, M. L., et al., 2022, A&A, 668, A109
Oba, Y., Takano, Y., Naraoka, H., et al., 2019, Nat. communications, 10, 1
Öberg, K. I., 2016, Chem. Rev., 116, 9631
Öberg, K. I., Boogert, A. C. A., Pontoppidan, K. M., et al., 2011, ApJ, 740, 109
Öberg, K. I., Fuchs, G. W., Awad, Z., et al., 2007, ApJ, 662, L23
Palumbo, M. E., Baratta, G. A., Fedoseev, G., et al., 2019, Proceedings of the International Astronomical Union, 15, 77
Pontoppidan, K. M., Boogert, A. C., Fraser, H. J., et al., 2008, ApJ, 678, 1005
Pontoppidan, K., 2006, A&A, 453, L47
Pontoppidan, K., Fraser, H., Dartois, E, et al., 2003, A&A, 408, 981
Pontoppidan, K., van Dishoeck, E., and Dartois, E, 2004, A&A, 426, 925
Preibisch, T., Ossenkopf, V, Yorke, H., et al., 1993, A&A, 279, 577
Qasim, D., Fedoseev, G., Chuang, K. J., et al., 2020, Nat. Astronomy, 4, 781
Rachid, M. G., Brunken, N., de Boe, D., et al., 2021, A&A, 653, A116
Rachid, M. G., Rocha, W., and Linnartz, H., 2022, A&A, 665, A89
Rachid, M. G., Terwisscha van Scheltinga, J., Koletzki, D., et al., 2020, A&A, 639, A4
Raut, U, Teolis, B., Loeffler, M., et al., 2007, J. Chem. Phys., 126, 244511
Rocha, W. R. M., Rachid, M. G., Olsthoorn, B., et al., 2022, A&A, 668, A63
Rocha, W. R., Perotti, G., Kristensen, L. E., et al., 2021, A&A, 654, A158
Rothard, H., Domaracka, A., Boduch, P., et al., 2017, Journal of Physics B: Atomic, Molecular and Optical Physics, 50, 062001
Saki, M., Gibb, E. L., Bonev, B. P., et al., 2020, Astronomical Journal, 160, 184
Schrödinger, E., 1926, Phys. Rev., 28, 1049
Schutte, W., Boogert, A., Tielens, A., et al., 1999, A&A, 343, 966

1.6. REFERENCES

Scirè, C, Urso, R., Fulvio, D, et al., 2019, Spectrochimica Acta Part A: Molecular and Biomolecular Spectroscopy, 219, 288

Sellgren, K., Werner, M. W., Ingalls, J. G., et al., 2010, ApJL, 722, L54

Snow, T. P. and McCall, B. J., 2006, ARA&A, 44, 367

Soifer, B., Puetter, R., Russell, R., et al., 1979, ApJ, 232, L53

Swings, P. and Rosenfeld, L., 1937, ApJ, 86, 483

Terwisscha van Scheltinga, J, Ligterink, N., Boogert, A., et al., 2018, A&A, 611, A35

Terwisscha van Scheltinga, J., Marcandalli, G., McClure, M. K., et al., 2021, A&A, 651, A95

Theulé, P, Duvernay, F, Danger, G., et al., 2013, Advances in Space Research, 52, 1567

Tielens, A. G. G. M. and Hagen, W., 1982, A&A, 114, 245

Tielens, A. G. G. M., 2008, ARA&A, 46, 289

Tsuge, M., Tseng, C.-Y., and Lee, Y.-P., 2018, PCCP, 20, 5344

Urso, R. G., Scirè, C., Baratta, G. A., et al., 2017, PCCP, 19, 21759

Whittet, D., Gerakines, P., Hough, J., et al., 2001, ApJ, 547, 872

Woolf, N. J. and Ney, E. P., 1969, ApJL, 155, L181

Yang, Y.-L., Bergner, J., Cleeves, I., et al. (Mar. 2021). *Blazing the trail of COMs from ice to gas.* JWST Proposal. Cycle 1, ID. #2151.

Yang, Y.-L., Green, J. D., Pontoppidan, K. M., et al., 2022, ApJL, 941, L13

Yang, Y.-L., Sakai, N., Zhang, Y., et al., 2021, ApJ, 910, 20

Zack, L. N. and Maier, J. P., 2014, Chemical Society Reviews, 43, 4602